Cancer Letters 519 (2021) 226–236

Contents lists available at ScienceDirect

Cancer Letters

journal homepage: www.elsevier.com/locate/canlet

MICAL1 regulates actin cytoskeleton organization, directional cell migration and the growth of human breast cancer cells as orthotopic xenograft tumours

David J. McGarry [a], Garett Armstrong [a], Giovanni Castino [a], Susan Mason [b], William Clark [b], Robin Shaw [b], Lynn McGarry [b], Karen Blyth [b,c], Michael F. Olson [a,d,*]

[a] Department of Chemistry and Biology, Ryerson University, Toronto, ON, Canada
[b] Cancer Research UK Beatson Institute, Glasgow, UK
[c] Institute of Cancer Sciences, University of Glasgow, Glasgow, UK
[d] Department of Pharmacology and Toxicology, University of Toronto, Toronto, ON, Canada

ARTICLE INFO

Keywords:
Cytoskeleton
Reactive oxygen species
cell morphology
cell motility
cell size
Transcription
Breast cancer
MICAL1

ABSTRACT

The *M*olecule *I*nteracting with *CasL* 1 (MICAL1) monooxygenase has emerged as an important regulator of cytoskeleton organization *via* actin oxidation. Although filamentous actin (F-actin) increases MICAL1 monooxygenase activity, hydrogen peroxide (H_2O_2) is also generated in the absence of F-actin, suggesting that diffusible H_2O_2 might have additional functions. *MICAL1* gene disruption by CRISPR/Cas9 in MDA MB 231 human breast cancer cells knocked out (KO) protein expression, which affected F-actin organization, cell size and motility. Transcriptomic profiling revealed that *MICAL1* deletion significantly affected the expression of over 700 genes, with the majority being reduced in their expression levels. In addition, the absolute magnitudes of reduced gene expression were significantly greater than the magnitudes of increased gene expression. Gene set enrichment analysis (GSEA) identified receptor regulator activity as the most significant negatively enriched molecular function gene set. The prominent influence exerted by MICAL1 on F-actin structures was also associated with changes in the expression of several serum-response factor (SRF) regulated genes in KO cells. Moreover, *MICAL1* disruption attenuated breast cancer tumour growth *in vivo*. Elevated *MICAL1* gene expression was observed in invasive breast cancer samples from human patients relative to normal tissue, while *MICAL1* amplification or point mutations were associated with reduced progression free survival. Collectively, these results demonstrate that *MICAL1* gene disruption altered cytoskeleton organization, cell morphology and migration, gene expression, and impaired tumour growth in an orthotopic *in vivo* breast cancer model, suggesting that pharmacological MICAL1 inhibition could have therapeutic benefits for cancer patients.

1. Introduction

The metastatic spread of cancer cells from primary tumours to distant sites is the deadliest aspect of the disease, estimated to contribute to ~90 % of solid cancer deaths [1]. The development of secondary tumours is often life threatening due to the loss of function of critically important tissues and organs, and because of limited effective treatment options following cancer cell dissemination. While the most efficacious cancer therapies are aided by early detection and removal of primary tumours before they become metastatic, many aggressive cancers such as breast, melanoma, pancreatic and lung [2–5] are often able to invade into lymphatic and blood vasculature systems before primary tumours are detected. Although conventional chemotherapies do not distinguish between tumour and healthy normal cells, resulting in toxic side effects, cancer selectivity may be achieved by targeting proteins that have prominent roles in the growth and progression of tumours, including proteins that contribute to cancer cell invasion and metastasis.

Metastasis is a multi-step process driven by the dynamic reorganization of the actin-myosin cytoskeleton [6]. Given that the cytoskeleton has essential roles in many fundamental processes [7], therapeutic drugs that directly target microfilaments have limited clinical utility due to their adverse impact on normal cell health. Alterations in the activity of

* Corresponding author. Ryerson University, 350 Victoria Street, Toronto, ON, M5B 2K3, Canada.
E-mail address: Michael.olson@ryerson.ca (M.F. Olson).

https://doi.org/10.1016/j.canlet.2021.07.039
Received 9 February 2021; Received in revised form 19 July 2021; Accepted 22 July 2021
Available online 24 July 2021

proteins that regulate cytoskeleton organization can influence the adhesive and invasive properties of tumour cells, as well as their proliferation and survival [8]. As a result, considerable effort has been focussed on identifying cytoskeleton regulators that are co-opted, mutated or differentially expressed in tumours because of their potential as cancer therapeutic targets [9].

Extracellular signals initiate the recruitment of protein complexes that catalyze the polymerization of actin monomers into filaments at cell leading edges [10]. The same extracellular signals trigger processes that contribute to F-actin severing or depolymerization, separated spatially and/or temporally from the actin polymerization machinery to enable dynamic reorganization of cytoskeleton structures. There is a growing body of evidence demonstrating that reactive oxygen species (ROS) act as important intermediary signalling molecules that regulate cellular pathways and processes that play prominent roles in cancer. ROS, such as hydrogen peroxide (H_2O_2), oxidize amino acid side chain thiols on proteins, producing oxidative intermediates and disulphide modifications [11]. These post-translational modifications have dramatic consequences on thiol structure that can result in changes in protein activity and localization [12]. ROS have been found elevated in many cancer types and can activate several signal transduction pathways that promote cellular growth and proliferation [13] [14]. In particular, there appears to be a close relationship between ROS generation and remodelling of the actin cytoskeleton to promote cancer motility and invasion [15,16]. Several known actin-binding proteins have previously been identified as being redox sensitive [17], and actin itself contains a number of reactive methionine residues that are subject to post-translational thiol modifications [18]. We previously discovered that H_2O_2 generation at the leading edge of migrating cells promotes the motility of invasive breast cancer cells through the oxidation, and subsequent inhibition, of the actin-severing protein cofilin1 [17]. Cofilin1 oxidation on cysteines 139 and 147 reduced its actin-binding and severing activities, while expression of oxidation-resistant cofilin1 mutants in cells inhibited cell spreading, and adhesion, and reduced the directionality of random migration relative to the expression of wild-type cofilin1. An outstanding question that emerged from those studies was the source of H_2O_2 at the leading edge of polarized migrating cells.

A significant cellular source of ROS production comes from the NADPH/DUOX oxidases (NOX/DUOX) and the recently described MICAL enzymes. NOX/DUOXs are a family of transmembrane flavoproteins that generate high levels of superoxide (or H_2O_2 depending on the isoform), and play diverse roles in cell physiology [19]. The cytoplasmic *Molecule Interacting with CasL* (MICAL) family proteins are flavo-monooxygenases that either directly oxidize bound proteins such as actin, or generate diffusible H_2O_2 that can oxidize nearby proteins such as collapsin response mediator protein-2 (CRMP2) [20]. The most well-defined function of the archetypal family member MICAL1 is F-actin depolymerization [21], which has important cell-specific roles including axon guidance and synapse development in neurons [22], and macrophage function [18]. MICAL1 regulation of F-actin structures is also important for successful cytokinesis in a variety of cell types [23].

To identify the H_2O_2 generating enzyme that influenced MDA MB 231 triple negative human breast cancer cell migration, we used CRISPR/Cas9 to knockout (KO) the *MICAL1* gene that we had determined to be the most highly expressed non-nuclear NOX/DUOX or MICAL family protein. We found that *MICAL1* KO had significant effects on F-actin organization, which were associated with increased two-dimensional cell areas and three-dimensional cell volumes without significantly affecting cell shape. Consistent with MICAL1 regulating cytoskeleton structures, the random migration of *MICAL1* KO cells was less directional, resulting in reduced forward distances being travelled over time. In addition, *MICAL1* KO cells closed gaps less efficiently in scratch wound healing assays. Gene expression analysis by RNA sequencing revealed that over 700 genes were significantly altered in *MICAL1* KO cells relative to control cells, with more genes being reduced in their expression compared to the number that were increased. In addition, the absolute magnitudes of reduced gene expression were significantly greater than the magnitudes of increased gene expression, and transcription factor target gene sets were negatively enriched. A gene set associated with the regulation of receptor activity was significantly negatively enriched in *MICAL1* KO cells, as were several genes regulated by the actin-responsive serum-response factor (SRF) transcription factor. Growth of *MICAL1* KO cells as orthotopic xenograft tumours in immunocompromised mice was significantly reduced relative to control cells. A role for *MICAL1* in human breast cancer was supported by results from publicly available databases, which revealed increased *MICAL1* expression in invasive breast cancers relative to normal mammary tissue and an association of *MICAL1* gene amplification or mutation with significantly reduced progression free survival. Taken together, these results demonstrate that MICAL1 is an important regulator of actin cytoskeleton organization, cell morphology and motility, gene transcription, and *in vivo* tumour growth of human breast cancer cells. The findings of this study suggest that MICAL1 is a potential drug target for breast cancer chemotherapy, future research will determine if other cancer types could also benefit from MICAL1 inhibition.

2. Materials and methods

2.1. Cell culture

MDA MB 231 and HEK293T cells were grown in DMEM (Sigma) supplemented with 10 % fetal bovine serum (FBS), 10 U/ml penicillin and 10 μg/ml streptomycin (Gibco). Cell line authentication was validated using STR profiling by the Cancer Research UK Beatson Institute Molecular Services, and cells were routinely tested for mycoplasma contamination. CRISPR/Cas9-mediated *MICAL1* knockouts were generated using the lentiCRISPR plasmid as previously described [24]. Target sequences for *MICAL1* are shown in Fig. S1A.

2.2. RNA isolation and qPCR

RNA and cDNA were isolated and prepared from MDA MB 231 cells as previously described [25]. Briefly, 5 x 10^5 cells were seeded onto 6 cm culture dishes and grown for 48 h. Cells were washed in PBS, and RNA was isolated using RNAeasy kits (Qiagen) according to the manufacturer's instructions. For RT-PCR reactions, cDNA was prepared using Quantitect Reverse Transcription kits (Qiagen). For gene expression analysis of *NOX1-5*, *DUOX1-2* and *MICAL1* (Fig. 1A), qPCR reactions were performed using QuantiTect primers (Qiagen) as follows; *NOX1* (QT00025585), *NOX2* (QT00029533), *NOX3* (QT00044737), *NOX4* (QT00057498), *NOX5* (QT00021924), *DUOX1* (QT00038346), *DUOX2* (QT00012236), *MICAL1* (QT00008421). For validation of targets from RNAseq analysis (Fig. 4E), qPCR reactions were performed using KiCq-Start® SYBR® Green kits (Sigma), with the following primer pairs; *RHOB* (5′-aaattttctctgcacctctg, 5′-gctcaccattttgtcatttg), SDC2 (5′-aaagtcacctgaagaaactg, 5′-agactgtctgagtgtttctc), CYR61 (5′-ttgattgcagttggaaaagg, 5′-gccttgtaaagggttgtatag). In all experiments, melting curves were generated to ensure the presence of a single PCR product for each primer. Gene expression data were calculated using ΔCt and normalized against *GAPDH*.

2.3. Immunoblotting

Immunoblots were performed as previously described [26]. Cells were washed thoroughly with ice cold PBS and lysed in buffer containing 1 % SDS, 50 mM Tris pH 7.5. Lysates were clarified at 13,000 rpm for 15 min and protein content measured using a BCA assay. Lysates (10 μg) were resolved on 4–12 % NuPAGE Bis-Tris gel and transferred to nitrocellulose membranes. Membranes were incubated with the following primary antibodies; anti-MICAL1 (Proteintech, 14818-1-AP), GAPDH (Millipore, MAB374), Cas9 (Diagenode, C15200203) and

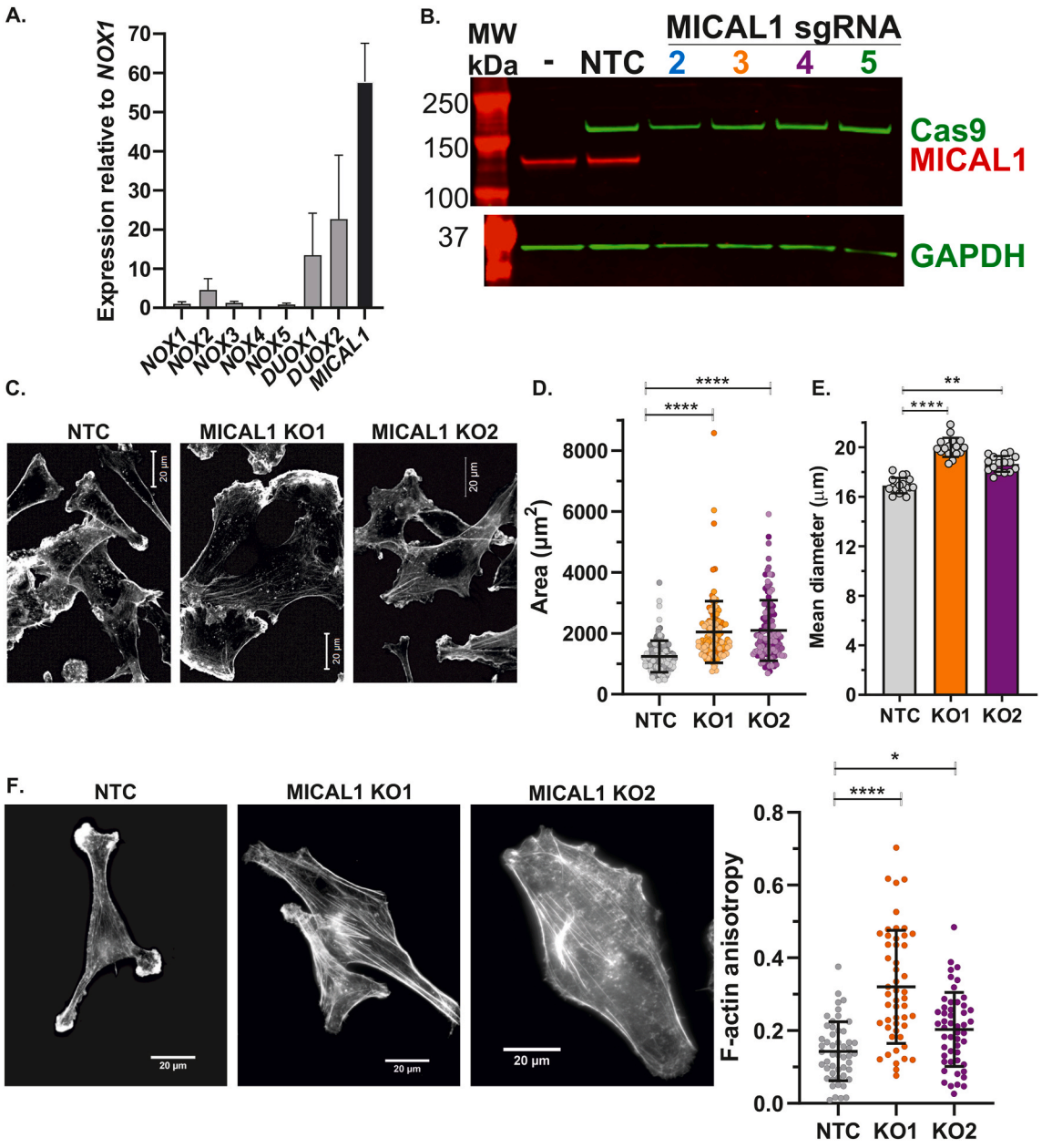

Fig. 1. *MICAL1* gene disruption affects cell size and actin organization. A. Expression of *NOX1-5*, *DUOX1&2* and *MICAL1* in MDA MB 231 cells as determined by RT-PCR. Means ± SD relative to mean expression of NOX1, n = 3 independent replicates. **B.** Validation of *MICAL1* knockout in MDA MB 231 cells by Western blot analysis of untreated cells (−), non-targeting control (NTC) and 4 independent sgRNA (2–5) targeted isolates **C.** Confocal microscopy images of phalloidin staining of fixed NTC or *MICAL1* KO cells. Scale bars = 20 µm. **D.** MDA MB 231 NTC and *MICAL1* KO cell areas (μm^2) were measured by high content imaging. Means ± SD, n = 120 individual cells imaged in 3 independent replicate experiments, indicated by the differing shading of each symbol. **** = $p < 0.0001$ (one-way ANOVA with *post-hoc* Dunnett's multiple comparisons test). **E.** Mean diameters (µm) of suspended NTC and *MICAL1* KO cells. Means ± SD, n = 19 (NTC), 20 (KO1) and 18 (KO2) independent determinations, with >5000 cells counted per replicate. **** = $p < 0.0001$ (one-way ANOVA with *post-hoc* Dunnett's multiple comparisons test) **F.** *Left panels;* TIRF images of phalloidin stained NTC and *MICAL1* KO MDA MB 231 cells. Scale bars = 20 µm. *Right panel;* F-actin anisotropy of phalloidin stained NTC and *MICAL1* KO MDA MB 231 cells. Means ± SD, n = 50 individual cells. **** = $p < 0.0001$, * = $p < 0.05$, (one-way ANOVA with *post-hoc* Dunnett's multiple comparisons test *t*-test relative to NTC condition).

secondary antibodies; IRDye® 680RD and 800CW (LiCor). Proteins were visualized by infrared imaging using LiCor Odyssey CLx.

2.4. Fluorescence microscopy

MDA MB 231 cells were grown on glass cover slips in 24 well plates. The next day, cell medium was removed, and cells were fixed with 4 % paraformaldehyde/PBS for 15 min at room temperature, then washed three times in PBS. For immunofluorescence, cells were permeabilized with 0.5 % Triton X-100/PBS for 5 min and washed with PBS. Cells were blocked with 1 % BSA/PBS for 30 min before being incubated with Alexa Fluor 488-conjugated phalloidin (Thermo Fisher, A12379). Images were taken using a Zeiss 710 upright confocal microscope.

2.5. Cell areas and diameters

Cell areas were analyzed as described previously [27]. Cells were fixed with 4 % paraformaldehyde/PBS in 96 well black plates and permeabilized with 0.5 % Triton X-100/PBS for 5 min at room temperature. After blocking with 1 % BSA/PBS, cells were stained with Cellomics®

Whole Cell Stain (Thermo Fisher Scientific, 8303401) for 30 min and 0.15 μg/ml DAPI (Sigma, D9542) for 20 min. Images were taken using an Operetta high-content imaging system, and data analyzed using the Columbus™ Analysis System (PerkinElmer). Mean diameter measurements were determined using a CASY® Cell Counter as described in Ref. [27]. For each independent mean diameter determination, >5000 cells were counted per replicate determination.

2.6. TIRF microscopy and F-actin anisotropy

Total internal reflectance (TIRF) images of phalloidin stained cells were taken using a Diskovery Multi-Model Imaging System (Quorum). Samples were prepared as described for fluorescence microscopy. Analysis of F-actin anisotropy was performed using the image J plugin FibrilTool [28].

2.7. Cell motility and morphology

MDA MB 231 cells were seeded at 1500 cells per well in 96 well ImageLock plates (Sartorius) and left for 24 h. Cells were treated with Incucyte Nuclight Rapid Red Dye (Sartorius), according to the manufacturer's protocol, and imaged every 10 min for 18 h in an IncuCyte S3 instrument (Sartorius) using a 10X objective. Time lapse images were imported into ImageJ2, and tracking files were generated using TrackMate as per the developer's protocol. Manual cell masking of eighth hour time lapse images (08h00 m) was completed in ImageJ to segment individual cell bodies, which were measured for size and shape using CellProfiler analysis software.

2.8. siRNA transfection

BT549 and SUM149PT cells were grown at 5 x 10^4 cells per well in 6 well plates. After 24 h, cells were transfected with siRNA using Lipofectamine RNAiMax (ThermoFisher), according to the manufacturer's instructions. ON-TARGETplus NTC and MICAL1 siRNAs were purchased from Dharmacon and used at 20 nM. After transfection, cells were incubated for 48 h before being washed, trypsinized, and seeded at 1 x 10^3 cells per well in Essen Bioscience ImageLock 96 well plates. Cells were imaged as described in the Cell Motility methods section.

2.9. Scratch wound migration assay

Cell migration was measured using the IncuCyte® S3 Live-Cell System [29]. Cells were seeded at 2 x 10^4 per well of Essen Bioscience ImageLock 96 well plates such that they formed confluent monolayers the next day. A wound was created using the IncuCyte® Woundmaker Tool. Cells were washed 3 times in full medium, then placed into the IncuCyte® S3 chamber. Brightfield images of the wells were taken every 2 h for a total of 48 h and wound width measured using the IncuCyte® S3 software.

2.10. RNA-sequencing and analysis

RNA-sequencing and analysis was performed as previously described [25]. RNA was isolated as described above for RT-PCR analysis, with the addition of on-column DNase digestion.

2.11. Mouse breast cancer model

Animal studies were performed in accordance with the UK Home Office regulations, in line with the Animals (Scientific Procedures) Act 1986, and approved by the University of Glasgow College of Medicine, Veterinary and Life Sciences Research Ethics Committee. All experiments were carried out under UK Home Office project licence authority (70/8645; held by KB) in dedicated barriered animal care facilities. MDA MB 231 control or *MICAL* KO cells (1x10^6) in 50 μl of 50 % Matrigel were transplanted to the inguinal (#4) mammary fat pads of 9 week CD1$^{nu/nu}$ immunocompromised female mice (Charles River Ltd, UK). Tumours were calliper measured and volumes calculated using the formula (Length x width^2)/2. Mice were euthanized when tumours reached 10 mm in diameter or after 86 days.

3. Results

3.1. MICAL1 disruption in MDA MB 231 cells

To identify potential sources of H_2O_2 that could facilitate cell motility, we profiled the expression of non-nuclear ROS generating enzymes by RT-PCR and found that the expression of *MICAL1* was greater than *NOX1-5* and *DUOX1-2* enzymes in MDA MB 231 cells (Fig. 1A). CRISPR/Cas9 technology was used with single guide RNAs (sgRNAs) that were designed to target exon 2 or exon 3 of the *MICAL1* gene to generate *MICAL1* knockout (KO) MDA MB 231 cell lines (Fig. S1A). Polyclonal expansion of lentivirus-transduced CRISPR/Cas9 KO cells avoided the risk of selecting individual subcellular populations from monoclonal expansions. As shown in Fig. 1B and Fig. S1B, MICAL1 was successfully knocked-out with multiple sgRNAs that targeted exon 2 or exon 3, while the non-targeting control (NTC) construct did not affect MICAL1 protein despite Cas9 expression. For subsequent studies, we selected *MICAL1* KO cell lines generated with the exon 3 targeted sgRNA3 (KO1) and the exon 2 targeted sgRNA4 (KO2).

3.2. MICAL1 knockouts alter the size of MDA MB 231 cells

The most well-defined function of MICAL1 is the oxidation of actin on Met44 and Met47, resulting in actin depolymerization and alterations to the organization of the actin cytoskeleton [21]. Using MDA MB 231 breast cancer *MICAL1* KO cells, we assessed whether MICAL1 loss altered cellular morphological properties that could arise from changes in cytoskeleton organization. Confocal microscope images of phalloidin-stained MDA MB 231 cells showed obvious changes in cell size (Fig. 1C). Quantification of mean two-dimensional areas of adherent cells (Fig. 1D and Fig. S2) or mean diameter of cells in suspension (Fig. 1E) revealed that *MICAL1* KO cells were significantly larger. Consistent with these changes, specific morphological parameters that are functionally related to altered cell size were significantly different in both KO1 and KO2 cells relative to the NTC control cells, including maximum (Fig. S3A), median (Fig. S3B) and mean radius (Fig. S3C), perimeter (Fig. S3D), and major (Fig. S3E) and minor axis lengths (Fig. S3F). In contrast, unitless relative parameters that relate to cell shape were unaffected by MICAL1 knockout, including cell eccentricity (Fig. S3G), area shape extent (Fig. S3H) and area shape form factor (Fig. S3I). To quantify differences in F-actin organization, total internal reflectance microscopy (TIRF) was used to reveal F-actin structures along a ~0.2 μm plane at cell-substrate interfaces (Fig. 1F, left panels), to eliminate possible effects of cell height differences. F-actin structures can be described as anisotropic if the organization is directionally biased, or isotropic when filament distribution is uniform in all directions. TIRF images were analyzed for F-actin anisotropy [28], which revealed that MDA MB 231 *MICAL1* KO cells had significantly increased F-actin anisotropy relative to NTC cells (Fig. 1F, right panel). These results demonstrate that disruption of *MICAL1* in MDA MB 231 cells led to cell size changes associated with alterations to the organization of the actin cytoskeleton.

3.3. MICAL1 disruption affects cell motility

We previously determined that MDA MB 231 cells selected on their ability to pass through 3 μm diameter micropores were more motile that unselected parental cells, which was associated with decreased F-actin anisotropy and smaller cell size [27]. Given that *MICAL1* KO resulted in increased cell size and F-actin anisotropy (Fig. 1), we sought to

determine whether *MICAL1* deletion would also affect cell motility. The random migration of individual NTC and *MICAL1* KO cells were tracked over 18 h. As shown in Spider cell track plots in Fig. 2A, *MICAL1* KO markedly reduced cell motility. Quantification of these individual cell tracks revealed that *MICAL1* deletion resulted in significantly ≥16 % reduced track displacement (Fig. 2B). The decreased forward progression was associated with lower directional persistence of migration as measured by the confinement ratio between the track displacement and the accumulated distance travelled (Fig. 2C). We additionally examined the requirement of MICAL1 for directional migration across 2-dimensional (2D) surfaces. MDA MB 231 NTC and *MICAL1* KO cell monolayers were grown to confluence before scratch wounds were created. The ability of cells to migrate into the open wounds was monitored over a 36 h period and wound widths measured using an Incucyte® S3 Live-Cell Analysis System every 2 h. Consistent with their decreased directional random cell migration (Fig. 2B and C), *MICAL1* KO cells moved more slowly into the scratched wounds (Fig. 2D). These observations support the conclusion that MICAL1 has an important role in enabling efficient and persistent cell motility.

To determine if there was a comparable role for MICAL1 in breast cancer cell motility, *MICAL1* expression was knocked down in BT549 and SUM149PT triple negative metastatic breast cancer cells using

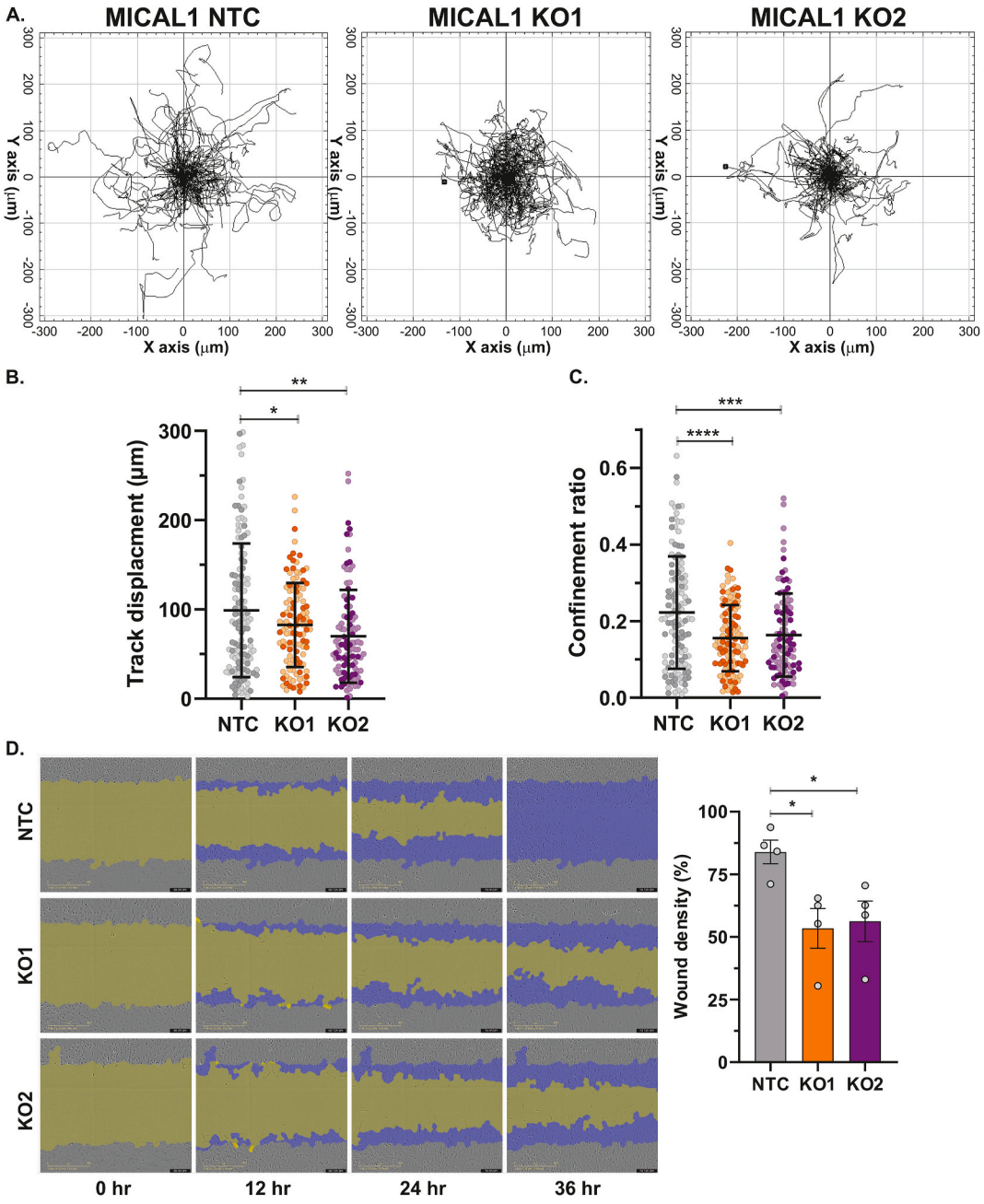

Fig. 2. *MICAL1* knockout reduces MDA MB 231 cell motility. A. Spider track plots showing single cell trajectories of NTC and *MICAL1* KO MDA MB 231 cells from a representative experiment. **B.** Single cell random migration track displacement (μm) and **C.** confinement ratios for) NTC and *MICAL1* KO MDA MB 231 cells. Means ± SD, n = 125 (NTC), n = 117 (KO1) and n = 103 individual cells from two independent experiments indicated by differing symbol shading. * = $p < 0.05$, ** = $p < 0.01$ (two tailed unpaired Student's t-test relative to NTC condition) **D.** Two-dimensional scratch wound assay of cells migrating into open wounds over 36 h. The areas of initial open wound are highlighted in yellow, and the proportion of cells that migrated into the wound from baseline are highlighted in purple. Scale bar = 400 μm. **E.** Relative cell densities in previously wounded areas of NTC and *MICAL1* KO cells after 36 h. Means ± SEM, n = 4 independent replicates. * = $p < 0.05$ (one-way ANOVA with *post-hoc* Dunnett's multiple comparisons test relative to NTC condition).

small-interfering RNA (siRNA; Fig. 3A and S4). Similar to the effect of *MICAL1* knockout (Fig. 2), knockdown of *MICAL1* significantly decreased random cell migration track displacements (Fig. 3B) in both cell lines. In addition, *MICAL1* knockdown also significantly reduced the directional persistence of migration by BT549 cells (Fig. 3B). The low confinement ratio for SUM149PT cells is indicative of their relatively inability to directionally migrate (Fig. 3C). Nonetheless, *MICAL1* knockdown did have some small effect at reducing their directional persistence of migration, albeit not significantly (Fig. 3C). These results support a general role for MICAL1 in promoting breast cancer cell migration.

3.4. Changes in gene transcription associated with MICAL1 deletion

Changes to the actin cytoskeleton may result in altered patterns of gene expression due to roles in regulating a variety of transcription factors [30], including direct influence on the activity of the serum-response factor (SRF) working together with the actin-binding myocardin-related transcription factors (MTRF) [31]. In parallel, cytoskeleton tension is sensed by the mechanoresponsive YAP/TAZ transcriptional co-activators [32]. There also are numerous transcription factors that are responsive to ROS, including Nuclear factor E2 related factor (Nrf2) [33], β-catenin [34–36], Forkhead box O (FOXO) family members [37,38], Nuclear Factor κB [39] and nuclear factor of activated T cells (NFAT) [40]. The transcriptomic responses induced by alterations to the cytoskeleton or changes in ROS levels could result in programmatic changes in gene sets that are linked with specific biological processes. Thus, MICAL1 might have effects on gene expression mediated both *via* actin-dependent and independent pathways. To assess the influence of MICAL1 on transcription regulation, polyA$^+$-enriched RNA was isolated from MDA MB 231 *MICAL1* KO or NTC cells and subjected to RNA sequencing (RNA-seq) analysis as we previously described [25,41]. Using cut-offs of greater than 1.5 fold change (FC) and adjusted P values (p_{adj}) less than 0.05, 749 of the 25032 genes sequenced (3.0 %) were found to be expressed at significantly differing levels between NTC and *MICAL1* KO cells (Fig. 4A). Overall, there were more genes expressed at lower levels in *MICAL1* KO cells, with 398 genes having decreased expression (average = −5.42 ± 10.3, median = −2.66 FC for KO1; average = −3.43 ± 6.42, median = −2.22 FC for KO2; Fig. 4B, red dots) and 351 genes with increased expression (average = 2.71 ± 1.67 FC, median = 2.15 FC for KO1; average = 2.13 ± 0.96, median = 1.81 FC for KO2; Fig. 4B, green dots), resulting in an overall significant reduction of total gene expression (Fig. 4B).

To characterize the types of molecular functions influenced by MICAL1, Gene Set Enrichment Analysis (GSEA) was performed on the RNAseq data [42]. Using false discovery rate (FDR) as a means to rank the gene sets least likely to be false positive findings, there were no positively enriched gene sets (FDR < 25 %) and one negatively enriched gene set from the 1708 Gene Ontology Molecular Function gene sets. The negatively enriched gene set was "receptor regulator activity", composed of genes associated with binding to and modulating receptor activity such as secreted signalling proteins (Fig. 4C). To characterize the global effect of MICAL disruption on transcription factor activity, the RNAseq data were compared to the 1133 transcription factor target gene sets. There were no transcription factor gene sets positively enriched using an FDR <25 % cut-off, and 14 gene sets significantly negatively enriched (Supplemental Table 1), indicating that the greatest effect of MICAL1 KO was on reducing transcription factor activity, in agreement with the significantly greater effect on decreasing gene transcript levels (Fig. 4B).

To determine if the effects on F-actin structures shown in Fig. 1F were associated with changes in the expression of SRF-regulated genes, we examined the expression patterns in MDA MB 231 NTC and *MICAL1* KO cells of 960 genes previously defined as being transcriptionally regulated by SRF [43]. MDA MB 231 cells detectably expressed 819 of the 960 SRF-regulated genes (85 %), of which 24 were significantly altered in both KO cell lines (2.9 %; Fig. 4D). To validate the observed effects on selected SRF-regulated genes identified as being significantly decreased in expression by RNAseq analysis, we performed quantitative RT-PCR (qPCR) using freshly isolated RNA from NTC and *MICAL1* KO cells and analyzed the expression of 3 exemplars (*RHOB, SDC2, CYR61*). As shown in Fig. 4E, all 3 genes were confirmed as being expressed at significantly reduced levels in *MICAL* KO cells.

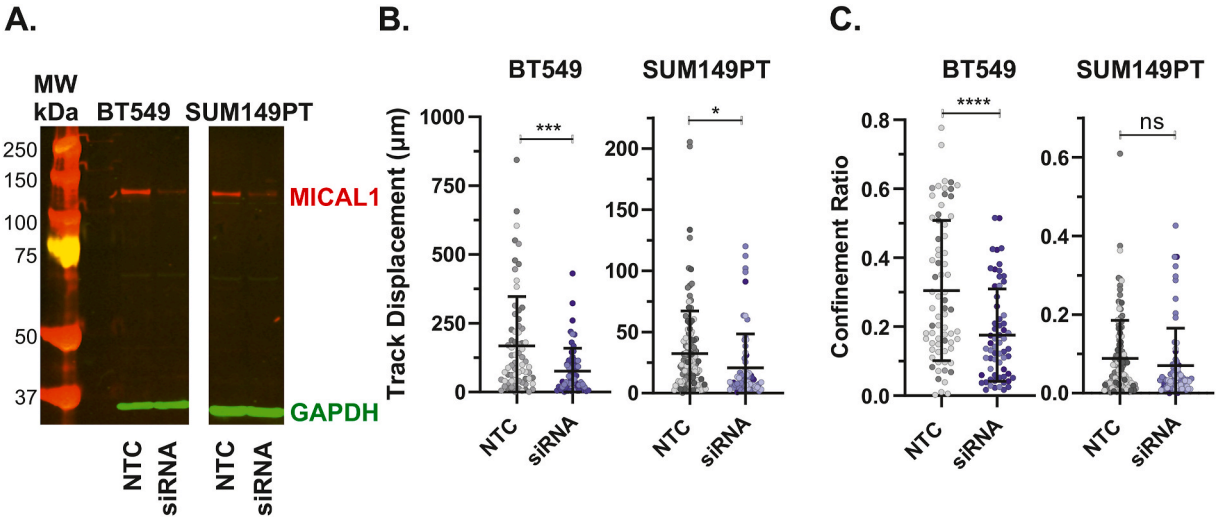

Fig. 3. *MICAL1* knockdown reduces BT549 and SUM149PT breast cancer cell motility. A. Western blot of MICAL1 and GAPDH expression in BT549 and SUM149PT cells following transfection with non-targeting control (NTC) or *MICAL1* targeted small interfering RNA (siRNA). **B.** Single cell random migration track displacement (μm) for BT549 (left graph) and SUM149PT (right graph). Means ± SD; BT549 n = 70 (NTC) and 63 (siRNA), SUM149PT n = 120 (NTC) and 70 (siRNA), from three (BT54) and four (SUM149) independent experiments indicated by differing symbol shading. *** = $p < 0.001$, * = $p < 0.05$ (one-way ANOVA with *post-hoc* Dunnett's multiple comparisons test relative to NTC condition). **C.** Single cell directional migration persistence as reflected by the confinement ratio of accumulated distance to total distance travelled for BT549 (left graph) and SUM149PT (right graph). Means ± SD; BT549 n = 70 (NTC) and 63 (siRNA), SUM149PT n = 120 (NTC) and 70 (siRNA), from three (BT54) and four (SUM149PT) independent experiments indicated by differing symbol shading. **** = $p < 0.0001$, ns = not significant (one-way ANOVA with *post-hoc* Dunnett's multiple comparisons test relative to NTC condition).

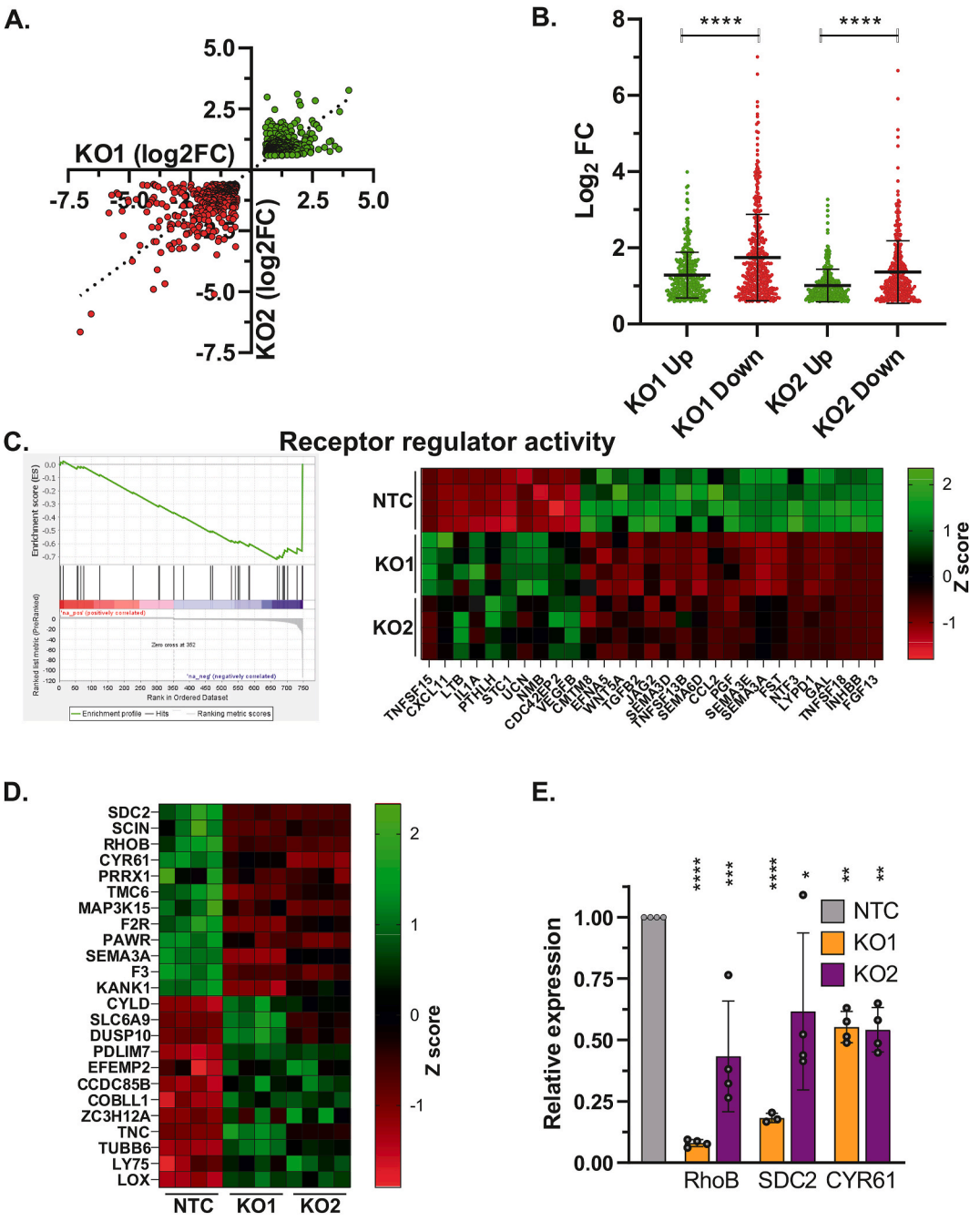

Fig. 4. RNA transcriptomic analysis of *MICAL1* KO cells. A. X–Y plot of $\log_2$ FC for 351 transcripts expressed ≥1.5 FC and $P_{adj} < 0.05$ in *MICAL1* KO1 and *MICAL1* KO2 cells relative to NTC cells (green dots), and 398 transcripts expressed ≥ 1.5 FC and $P_{adj} < 0.05$ in NTC relative to *MICAL1* KO1 and *MICAL1* KO2 cells (red dots). Deming regression shown by the dotted line indicates the line of best fit for the two-dimensional dataset. B. Scatter plot of $\log_2$ FC for 351 transcripts expressed ≥1.5 FC and $P_{adj} < 0.05$ in *MICAL1* KO1 and *MICAL1* KO2 cells relative to NTC cells (Up; green dots), and 398 transcripts expressed ≥ 1.5 FC and $P_{adj} < 0.05$ in NTC relative to *MICAL1* KO1 and *MICAL1* KO2 cells (Down; red dots). Means ± SD. **** = $p < 0.0001$ (two-tailed unpaired Student's t-test). **C.** *Left panel;* Gene set enrichment analysis (GSEA) enrichment plot for the gene set with a false discovery rate < 25 %. *Right panel;* Heat map of z scores for 4 independent replicate RNA sequence reads for indicated transcripts from NTC or *MICAL1* KO1 and KO2 cells. **D.** Heat map of z scores for 4 independent replicate RNA sequence reads for indicated SRF-regulated transcripts from NTC or *MICAL1* KO1 and KO2 cells. **E.** Validation of SRF gene expression in NTC and *MICAL1* KO cells by RT-PCR. For each transcript, expression was individually normalized to the levels in NTC cells, which has been depicted as a single grey bar. Means ± SD, n = 4 independent replicates. **** = $p < 0.0001$, *** = $p < 0.001$, ** = $p < 0.01$, * = $p < 0.05$ (one-way ANOVA with *post-hoc* Dunnett's multiple comparisons test relative to NTC condition).

3.5. *MICAL1 promotes cancer growth in vivo*

Disruption of MICAL1 expression in MDA MB 231 cells affected several cellular properties, including morphology, cell size, motility and gene expression (Figs. 1–4). We next sought to determine if MICAL1 contributed to the tumorigenic properties of these breast cancer cells in an *in vivo* orthotopic tumour model. MDA MB 231 NTC and *MICAL1* KO cells were injected as 10^6 cells suspended in 50 % Matrigel into the fourth abdominal mammary fat pads of female CD1-*nude* mice, then tumour dimensions were measured after they became palpable over 86 subsequent days (Fig. 5A). Tumours formed in 7/8 mice injected with NTC cells, and 4 mice were deemed to have reached their experimental endpoint and removed from the study in under 50 days due to tumours approaching or reaching maximally permitted tumour diameters of 10

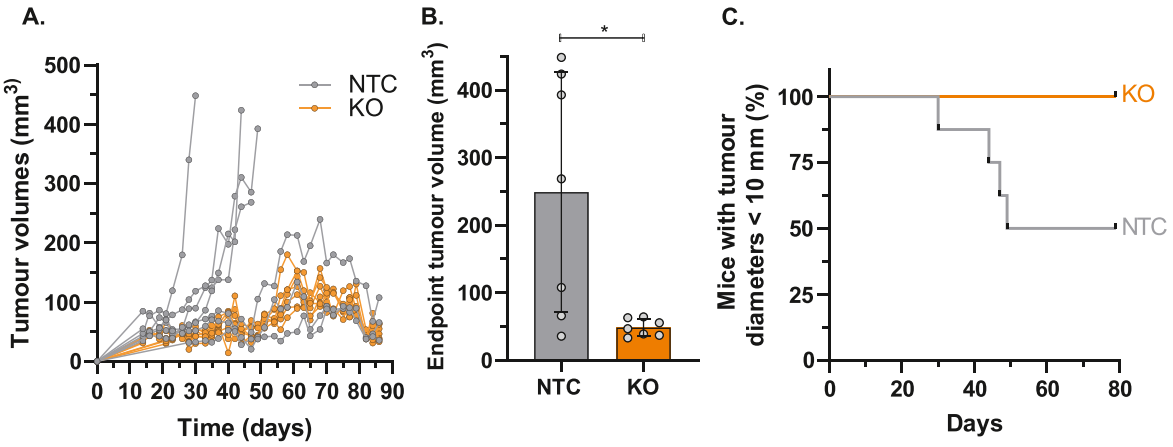

Fig. 5. *MICAL1* KO attenuates MDA MB 231 cell growth *in vivo*. A. MDA MB 231 NTC and *MICAL1* KO cells were injected into the mammary fat pads of 9 week old immunocompromised mice. Individual tumour volume (mm^3) curves for n = 7 NTC and n = 7 *MICAL1* KO tumours are shown up to 86 days post-injection. **B.** Tumour volumes (mm^3) at experimental endpoints, either study removal due to tumours reaching maximally permitted size or after 86 days post-injection. Means ± SD, n = 7. * = $p < 0.05$ (two-tailed unpaired Student's t-test). **C.** Kaplan-Meier curve showing the percentage of tumours removed once they reached maximally permitted size endpoint (>10 mm in diameter). N = 7.

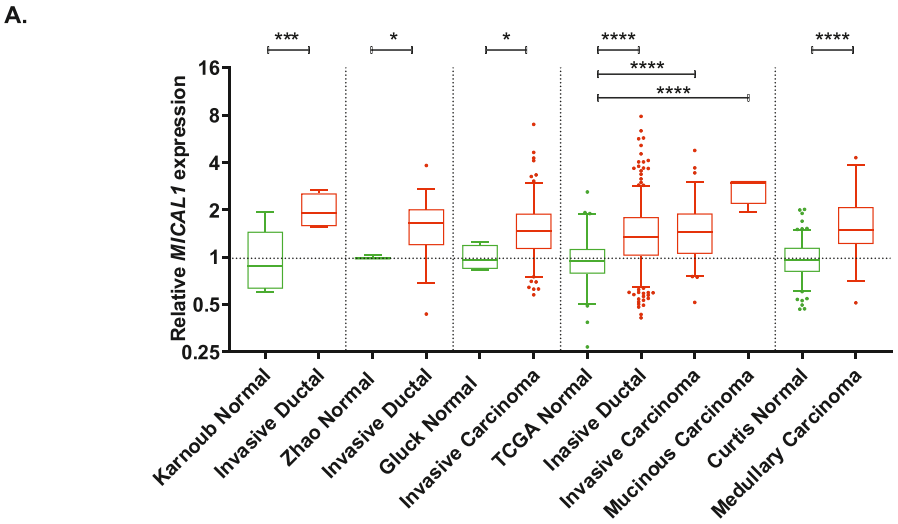

Fig. 6. *MICAL1* expression and genomic alterations in human breast cancer. A. Publicly available microarray data was analyzed using Oncomine [45], which revealed significantly higher expression in indicated breast cancers relative to normal control tissues. *MICAL1* expression was normalized to mean expression in normal tissue for each indicated study. Box indicates upper and lower quartiles and median, whiskers indicate 5–95 % range with outliers. Statistical significance was evaluated by two-tailed Mann-Whitney tests, **** = $p < 0.0001$; *** = $p < 0.001$; * = $p < 0.05$ **B.** Kaplan-Meier curves showing the probability of progression free survival for 1053 patients with invasive breast cancer with no *MICAL1* (blue line) alterations or 29 patients with *MICAL1* amplifications or mutations (red line). Statistical significance was evaluated by logrank test. Data from the 2018 TCGA pan-cancer atlas survey [50].

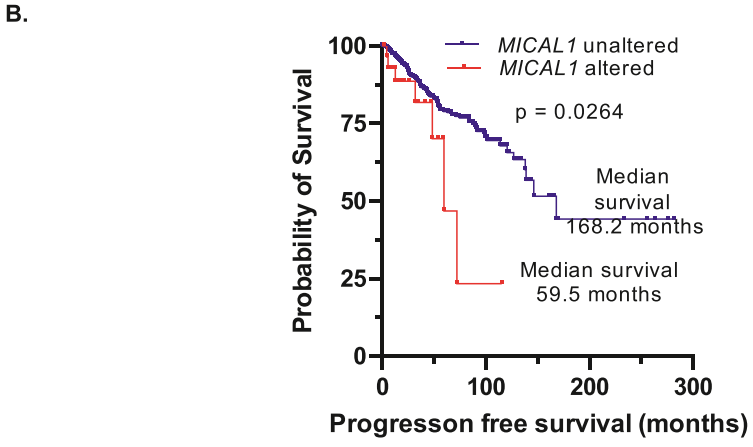

mm (Fig. 5A). For tumours derived from *MICAL* KO cells, 7/8 mice also formed tumours, none of which neared 10 mm in diameter even after 86 days (Fig. 5A) Using the formula of tumour volume = ½(length X width^2) [44] to compare tumour growth, the volumes of NTC tumours were significantly greater at experimental endpoints than those grown from injected *MICAL1* KO cells (Fig. 5B). Furthermore, when survival was plotted for *MICAL1* KO and NTC tumour bearing mice, there was obvious separation between the experimental groups (Fig. 5C). Together, these data demonstrate that MICAL1 contributes to cancer cell morphology, motility and gene expression *in vitro* and tumour growth *in vivo*.

Given the significant role that regulation of actin-myosin cytoskeleton dynamics has in cancer invasion and metastasis, we next assessed whether *MICAL1* alterations were associated with human breast cancer. Oncomine [45] analysis of publicly available microarray data provided evidence implicating increased *MICAL1* expression in multiple breast cancers such as medullary breast cancer, invasive ductal carcinoma and invasive breast carcinoma [46–49] (Fig. 6A). Furthermore, examining The Cancer Genome Atlas (TCGA) pan-cancer survey for *MICAL1* genetic alterations revealed that invasive breast cancer patients [50] with amplifications or mutations had significantly ($p = 0.0264$) reduced progression free survival (Fig. 6B). Taken together with the mouse xenograft cancer model data, these results indicate that MICAL1 makes an important contribution to breast cancer.

4. Discussion

MICAL family proteins are FAD binding multi-domain proteins that oxidize actin in a NADPH dependent manner [20]. Since their discovery ~20 years ago, MICAL proteins have been associated with several cellular process that are dependent on dynamic actin reorganization, such as neuronal development, endocytosis, cell division and abscission [51,52]. Initial work in *Drosophila* demonstrated that F-actin is a substrate for MICAL1, which oxidizes two methionine residues, Met44 and Met47, resulting in actin depolymerization [21]. Recent evidence indicates that MICAL1 does not directly sever filamentous actin, but weakens the links between actin subunits within polymerized filaments through methionine oxidation [21,23] and enhances the interaction with actin severing proteins such as cofilin1 [53]. These observations support a central and prominent role of MICAL proteins in cytoskeleton regulation.

Mesenchymal transformation of epithelial cells, including changes in shape, size, and motility, are prominent features of transformed cancer cells [54]. Central to these changes is reorganization of actin filaments that contribute to the dynamic generation of mechanical force required for cell migration and tumour cell metastasis [6]. As a result, signalling mechanisms controlling F-actin polymerization and depolymerization machinery play critical roles in cancer *via* their spatial and temporal regulation of the actin cytoskeleton. The cytoskeleton also provides a physical scaffold that connects extracellular stimuli with intracellular signalling events that promote tumour growth and progression. As a consequence, inhibition of proteins that regulate the actin cytoskeleton often result in decreased tumour growth and/or spread, as work from our laboratory demonstrated for *in vivo* cancer models using small molecule inhibitors of the ROCK [29,55,56], LIMK [56] and MRCK kinases [24,57], as well as inhibition of myosin ATPase activity [56].

Much of the historical research on MICAL proteins has focussed on their roles in normal cells, such that their roles in cancer are not well characterized. To determine how MICAL1 signalling contributed to the tumourigenic properties of human breast cancer cells, we used CRISPR/Cas9 to disrupt the *MICAL1* gene in MDA MB 231 cells, a triple negative metastatic mammary adenocarcinoma cell line [58]. Consistent with a direct role in regulating F-actin, *MICAL1* KO resulted in alterations to the organization of the actin cytoskeleton that were associated with increased cell size and reduced cell migration (Figs. 1 and 2). We previously observed that selection of MDA MB 231 cells for their ability to pass through narrow diameter microporous membranes led to the isolation of a sub-population with reduced F-actin anisotropy, smaller cell size and increased cell motility relative to the starting unselected population [27,59]. These observations reinforce the conclusion that F-actin organization, cell size and motility are inter-connected, and that the consequence of *MICAL1* gene disruption resulted in direct effects on actin organization that were consequently manifested in changes in cell morphology and motility.

Analysis of gene expression revealed that *MICAL1* gene disruption resulted in changes in the levels of over 700 genes, with the majority being reduced in their expression (Fig. 4). Similar to the previous observation that the nuclear-localized homologue MICAL2 influenced the expression of SRF/MTRF regulated genes via F-actin depolymerization [60], *MICAL1* KO significantly altered the expression of 24 SRF-regulated genes by at least 1.5-fold (Fig. 4). Given that the majority of the changes in expression were for genes not known to be regulated by SRF/MTRF, they were most likely influenced by actin-independent pathways. One possibility is that the absence of MICAL1 protein affected ROS-responsive mechanisms that contribute to transcriptional regulation.

To evaluate the relative importance of MICAL1 for breast cancer growth *in vivo,* control and *MICAL1* KO cells were grown as orthotopic xenograft tumours in immunocompromised mice (Fig. 5). While the tumour take of each experimental group was equivalent, 4/7 NTC control tumours grew so rapidly that they reached maximally permitted size endpoints in less than 50 days after injection. In contrast, none of the 7 MICAL KO tumours approached maximally permitted size, and all partially regressed after peaking in size 50–80 days after injection (Fig. 5A). Previous studies found that siRNA-mediated knockdown of MICAL1 expression in MCF-7 human breast adenocarcinoma cells reduced epidermal growth factor (EGF) stimulation of AKT signalling [61], and that MICAL1 knockdown in T47D human breast adenocarcinoma cells reduced basal mitogen-activated protein kinase (MAPK) signalling and slowed proliferation, which was attributed to decreased expression of Cyclin D1 [62]. Analysis of differences in gene expression between control and *MICAL1* KO cells revealed the only significant negatively enriched gene set as receptor regulator activity (Fig. 4C), suggesting that loss of MICAL1 expression may have pleiotropic effects on numerous signalling pathways. Attenuated growth factor signalling, resulting in decreased activity of important regulators of proliferation such as AKT and the MAPK pathway, would be predicted to negatively affect proliferation and tumour growth. These effects on growth factor activity and cellular signalling are likely due to changes in actin cytoskeleton structures that contribute to efficient signalling by acting as scaffolds and by promoting receptor trafficking, as well as through reduced ROS generation and transcription factor activity.

Evidence from human breast cancer patients also indicates a potential contribution of elevated *MICAL1* expression and activity, particularly associated with invasive and metastatic properties (Fig. 6A and B). Analysis of *MICAL1* expression in several studies showed increased levels relative to normal mammary tissue (Fig. 6A). The most common genomic alteration of the *MICAL1* gene is amplification, but the ~4 % incidence detected in retrospective studies of metastatic breast cancer [63] suggests that additional mechanisms make significant contributions to the observed increased expression levels, such as epigenetic alterations that promote efficient gene transcription. Although the incidence of *MICAL1* gene amplification is relatively low compared to the ~15 % incidence of *HER2* amplification that reflects HER2 signalling being a major cancer driver [64], the significant adverse effect on the progression-free survival of patients with *MICAL1* amplification relative to those without (Fig. 6B) suggests that MICAL1 does indeed positively contribute to breast cancer.

Additional validation studies will clarify the potential of MICAL1 as a *bona fide* chemotherapeutic target for breast cancer treatment, and will help to identify the sub-types most likely to benefit from therapy. MDA MB 231 breast cancer cells are a representative of triple-negative

invasive ductal adenocarcinoma that accounts for ~15 % of all breast cancers and which, have limited treatment options and very poor prognosis due to rapid growth and spread [65]. As a result, there is an urgent need to identify novel molecular targets that could be the focus of drug discovery efforts. Further research will also determine if there are additional cancer types and sub-types that are promoted by the actions of MICAL1. It also remains to be determined which of the actions of MICAL1 on cytoskeleton regulation, or as a source of ROS, make the greatest contribution to its tumour promoting actions. In support of the latter possibility, the reactive oxygen scavenger n-acetylcysteine has been proposed to have therapeutic benefit for the therapy of triple-negative breast cancer [66]. An advantage of directly inhibiting MICAL1 is that it would block both aspects of its biological activities, cytoskeleton regulation and ROS generation, thereby having the greatest potential effect.

CRediT authorship contribution statement

David J. McGarry: Conceptualization, Data curation, Formal analysis, Investigation, Methodology, Project administration, Visualization, Writing – original draft. **Garett Armstrong:** Data curation, Formal analysis, Investigation, Methodology, Visualization, Writing – original draft. **Giovanni Castino:** Data curation, Investigation, Methodology. **Susan Mason:** Data curation, Investigation, Methodology. **William Clark:** Investigation, Methodology, Resources. **Robin Shaw:** Data curation, Formal analysis, Methodology, Software. **Lynn McGarry:** Data curation, Formal analysis, Investigation, Methodology. **Karen Blyth:** Data curation, Resources, Supervision, Writing – review & editing. **Michael F. Olson:** Conceptualization, Data curation, Formal analysis, Funding acquisition, Project administration, Resources, Supervision, Visualization, Writing – original draft.

Declaration of competing interest

The authors declare that they have no competing financial interests that influenced the work reported in this paper.

Acknowledgements

We wish to thank the staff of the Biological Services facility at the Cancer Research UK (CRUK) Beatson Institute, funded by CRUK (A18076, A17196). This research was supported by CRUK institutional funding to the CRUK Beatson Institute (A10419, A17196), to the Blyth lab (A29799), and to the Olson lab (A18276). Additional funding to M.F. O from the Canadian Institutes of Health Research (PJT-169125), Natural Sciences and Engineering Research Council of Canada (RGPIN-2020-05388), Canada Research Chairs Program (950–231665), and the Ryerson University Faculty of Science Dean's Research Fund. Some of the results shown are in part based upon data generated by the TCGA Research Network: https://www.cancer.gov/tcga.

Appendix A. Supplementary data

Supplementary data to this article can be found online at https://doi.org/10.1016/j.canlet.2021.07.039.

References

[1] C.L. Chaffer, R.A. Weinberg, A perspective on cancer cell metastasis, Science 331 (6024) (2011) 1559–1564.
[2] C. Melzer, J. von der Ohe, R. Hass, Breast carcinoma: from initial tumor cell detachment to settlement at secondary sites, BioMed Res. Int. 2017 (2017) 8534371.
[3] J.J. Luke, et al., Targeted agents and immunotherapies: optimizing outcomes in melanoma, Nat. Rev. Clin. Oncol. 14 (8) (2017) 463–482.
[4] S. Yachida, et al., Distant metastasis occurs late during the genetic evolution of pancreatic cancer, Nature 467 (7319) (2010) 1114–1117.
[5] S. Blandin Knight, et al., Progress and prospects of early detection in lung cancer, Open Biol 7 (9) (2017).
[6] M.F. Olson, E. Sahai, The actin cytoskeleton in cancer cell motility, Clin. Exp. Metastasis 26 (4) (2009) 273–287.
[7] A. Hall, Rho GTPases and the control of cell behaviour, Biochem. Soc. Trans. 33 (Pt 5) (2005) 891–895.
[8] A. Gandalovičová, et al., Migrastatics-Anti-metastatic and anti-invasion drugs: promises and challenges, Trends Cancer 3 (6) (2017) 391–406.
[9] D. Rosel, et al., Migrastatics: redirecting R&D in solid cancer towards metastasis? Trends Cancer 5 (12) (2019) 755–756.
[10] E.F. Woodham, L.M. Machesky, Polarised cell migration: intrinsic and extrinsic drivers, Curr. Opin. Cell Biol. 30 (2014) 25–32.
[11] V. Gupta, K.S. Carroll, Sulfenic acid chemistry, detection and cellular lifetime, Biochim. Biophys. Acta 1840 (2) (2014) 847–875.
[12] B. Groitl, U. Jakob, Thiol-based redox switches, Biochim. Biophys. Acta 1844 (8) (2014) 1335–1343.
[13] J.D. Hayes, A.T. Dinkova-Kostova, K.D. Tew, Oxidative stress in cancer, Canc. Cell 38 (2) (2020) 167–197.
[14] C.R. Reczek, N.S. Chandel, The two faces of reactive oxygen species in cancer, Annu. Rev. Cell Biol. 1 (1) (2017) 79–98.
[15] V. Aggarwal, et al., Role of reactive oxygen species in cancer progression: molecular mechanisms and recent advancements, Biomolecules 9 (11) (2019).
[16] J.L. Meitzler, M.M. Konaté, J.H. Doroshow, Hydrogen peroxide-producing NADPH oxidases and the promotion of migratory phenotypes in cancer, Arch. Biochem. Biophys. 675 (2019) 108076.
[17] J.M. Cameron, et al., Polarized cell motility induces hydrogen peroxide to inhibit cofilin via cysteine oxidation, Curr. Biol. 25 (11) (2015) 1520–1525.
[18] B.C. Lee, et al., MsrB1 and MICALs regulate actin assembly and macrophage function via reversible stereoselective methionine oxidation, Mol. Cell. 51 (3) (2013) 397–404.
[19] K. Block, Y. Gorin, Aiding and abetting roles of NOX oxidases in cellular transformation, Nat. Rev. Canc. 12 (9) (2012) 627–637.
[20] S.S. Giridharan, S. Caplan, MICAL-family proteins: complex regulators of the actin cytoskeleton, Antioxidants Redox Signal. 20 (13) (2014) 2059–2073.
[21] R.J. Hung, C.W. Pak, J.R. Terman, Direct redox regulation of F-actin assembly and disassembly by Mical, Science 334 (6063) (2011) 1710–1713.
[22] E.F. Schmidt, S.O. Shim, S.M. Strittmatter, Release of MICAL autoinhibition by semaphorin-plexin signaling promotes interaction with collapsin response mediator protein, J. Neurosci. 28 (9) (2008) 2287–2297.
[23] S. Frémont, et al., Oxidation of F-actin controls the terminal steps of cytokinesis, Nat. Commun. 8 (2017) 14528.
[24] M. Unbekandt, et al., Discovery of potent and selective MRCK inhibitors with therapeutic effect on skin cancer, Canc. Res. 78 (8) (2018) 2096–2114.
[25] D.A. Rudzka, et al., Transcriptomic profiling of human breast and melanoma cells selected by migration through narrow constraints, Sci Data 4 (2017) 170172.
[26] D.J. McGarry, et al., A cell-permeable biscyclooctyne as a novel probe for the identification of protein sulfenic acids, ACS Chem. Biol. 11 (12) (2016) 3300–3304.
[27] D.A. Rudzka, et al., Migration through physical constraints is enabled by MAPK-induced cell softening via actin cytoskeleton re-organization, J. Cell Sci. 132 (11) (2019).
[28] A. Boudaoud, et al., FibrilTool, an ImageJ plug-in to quantify fibrillar structures in raw microscopy images, Nat. Protoc. 9 (2) (2014) 457–463.
[29] N. Rath, et al., Rho kinase inhibition by AT13148 blocks pancreatic ductal adenocarcinoma invasion and tumor growth, Canc. Res. 78 (12) (2018) 3321–3336.
[30] J. Seo, J. Kim, Regulation of Hippo signaling by actin remodeling, BMB Rep 51 (3) (2018) 151–156.
[31] G. Posern, R. Treisman, Actin' together: serum response factor, its cofactors and the link to signal transduction, Trends Cell Biol. 16 (11) (2006) 588–596.
[32] I. Dasgupta, D. McCollum, Control of cellular responses to mechanical cues through YAP/TAZ regulation, J. Biol. Chem. 294 (46) (2019) 17693–17706.
[33] J.M. DeBlasi, G.M. DeNicola, Dissecting the crosstalk between NRF2 signaling and metabolic processes in cancer, Cancers 12 (10) (2020).
[34] Y. Funato, et al., The thioredoxin-related redox-regulating protein nucleoredoxin inhibits Wnt-beta-catenin signalling through dishevelled, Nat. Cell Biol. 8 (5) (2006) 501–508.
[35] S. Kajla, et al., A crucial role for Nox 1 in redox-dependent regulation of Wnt-β-catenin signaling, Faseb. J. 26 (5) (2012) 2049–2059.
[36] N. Wang, et al., Activation of Wnt/β-catenin signaling by hydrogen peroxide transcriptionally inhibits NaV1.5 expression, Free Radic. Biol. Med. 96 (2016) 34–44.
[37] P. Storz, Forkhead homeobox type O transcription factors in the responses to oxidative stress, Antioxidants Redox Signal. 14 (4) (2011) 593–605.
[38] L.O. Klotz, et al., Redox regulation of FoxO transcription factors, Redox Biol 6 (2015) 51–72.
[39] R. Schreck, K. Albermann, P.A. Baeuerle, Nuclear factor kappa B: an oxidative stress-responsive transcription factor of eukaryotic cells (a review), Free Radic. Res. Commun. 17 (4) (1992) 221–237.
[40] C. Huang, et al., Vanadium-induced nuclear factor of activated T cells activation through hydrogen peroxide, J. Biol. Chem. 276 (25) (2001) 22397–22403.
[41] N. Rath, et al., ROCK signalling induced gene expression changes in mouse pancreatic ductal adenocarcinoma cells, Sci Data 3 (2016) 160101.
[42] A. Subramanian, et al., Gene set enrichment analysis: a knowledge-based approach for interpreting genome-wide expression profiles, Proc. Natl. Acad. Sci. U. S. A. 102 (43) (2005) 15545–15550.

[43] C. Esnault, et al., Rho-actin signaling to the MRTF coactivators dominates the immediate transcriptional response to serum in fibroblasts, Genes Dev. 28 (9) (2014) 943–958.
[44] A. Faustino-Rocha, et al., Estimation of rat mammary tumor volume using caliper and ultrasonography measurements, Lab. Anim. 42 (6) (2013) 217–224.
[45] D.R. Rhodes, et al., ONCOMINE: a cancer microarray database and integrated data-mining platform, Neoplasia 6 (1) (2004) 1–6.
[46] A.E. Karnoub, et al., Mesenchymal stem cells within tumour stroma promote breast cancer metastasis, Nature 449 (7162) (2007) 557–563.
[47] H. Zhao, et al., Different gene expression patterns in invasive lobular and ductal carcinomas of the breast, Mol. Biol. Cell 15 (6) (2004) 2523–2536.
[48] S. Glück, et al., TP53 genomics predict higher clinical and pathologic tumor response in operable early-stage breast cancer treated with docetaxel-capecitabine ± trastuzumab, Breast Canc. Res. Treat. 132 (3) (2012) 781–791.
[49] C. Curtis, et al., The genomic and transcriptomic architecture of 2,000 breast tumours reveals novel subgroups, Nature 486 (7403) (2012) 346–352.
[50] J. Liu, et al., An integrated TCGA pan-cancer clinical data resource to drive high-quality survival outcome analytics, Cell 173 (2) (2018) 400–416, e11.
[51] S. Frémont, et al., Emerging roles of MICAL family proteins - from actin oxidation to membrane trafficking during cytokinesis, J. Cell Sci. 130 (9) (2017) 1509–1517.
[52] L.T. Alto, J.R. Terman, *MICALs.* Curr Biol 28 (9) (2018) R538–r541.
[53] E.E. Grintsevich, et al., F-actin dismantling through a redox-driven synergy between Mical and cofilin, Nat. Cell Biol. 18 (8) (2016) 876–885.
[54] A. Dongre, R.A. Weinberg, New insights into the mechanisms of epithelial-mesenchymal transition and implications for cancer, Nat. Rev. Mol. Cell Biol. 20 (2) (2019) 69–84.
[55] N. Rath, et al., ROCK signaling promotes collagen remodeling to facilitate invasive pancreatic ductal adenocarcinoma tumor cell growth, EMBO Mol. Med. 9 (2) (2017) 198–218.
[56] M.S. Samuel, et al., Actomyosin-mediated cellular tension drives increased tissue stiffness and β-catenin activation to induce epidermal hyperplasia and tumor growth, Canc. Cell 19 (6) (2011) 776–791.
[57] J.L. Birch, et al., A novel small-molecule inhibitor of MRCK prevents radiation-driven invasion in glioblastoma, Canc. Res. 78 (22) (2018) 6509–6522.
[58] K.J. Chavez, S.V. Garimella, S. Lipkowitz, Triple negative breast cancer cell lines: one tool in the search for better treatment of triple negative breast cancer, Breast Dis. 32 (1–2) (2010) 35–48.
[59] D.A. Rudzka, et al., Selection of established tumour cells through narrow diameter micropores enriches for elevated Ras/Raf/MEK/ERK MAPK signalling and enhanced tumour growth, Small GTPases (2020) 1–17.
[60] M.R. Lundquist, et al., Redox modification of nuclear actin by MICAL-2 regulates SRF signaling, Cell 156 (3) (2014) 563–576.
[61] W. Deng, et al., MICAL1 controls cell invasive phenotype via regulating oxidative stress in breast cancer cells, BMC Canc. 16 (2016) 489.
[62] W. Deng, et al., MICAL1 facilitates breast cancer cell proliferation via ROS-sensitive ERK/cyclin D pathway, J. Cell Mol. Med. 22 (6) (2018) 3108–3118.
[63] C. Lefebvre, et al., Mutational profile of metastatic breast cancers: a retrospective analysis, PLoS Med. 13 (12) (2016), e1002201.
[64] U. Krishnamurti, J.F. Silverman, HER2 in breast cancer: a review and update, Adv. Anat. Pathol. 21 (2) (2014) 100–107.
[65] R. Schmadeka, B.E. Harmon, M. Singh, Triple-negative breast carcinoma: current and emerging concepts, Am. J. Clin. Pathol. 141 (4) (2014) 462–477.
[66] Y. Kwon, Possible beneficial effects of N-acetylcysteine for treatment of triple-negative breast cancer, Antioxidants 10 (2) (2021).